Supporting Information

A 'self-activating' Bi_3TaO_7-Bi_4TaO_8Br photocatalyst and its use in the sustainable production of pro-fluorophoric Rhodamine-110

Maqsuma Banoo,[‡1] Kaustav Chatterjee,[‡1] Sanjit Mondal,[1] C. P. Vinod,[2] Ujjal K. Gautam[*]

[1]Department of Chemical Sciences, Indian Institute of Science Education and Research (IISER)-Mohali, Sector 81, Mohali, SAS Nagar, Punjab 140306, India

[2]Catalysis and Inorganic Chemistry Division, CSIR-NCL, Pune 411008, India

([‡] equal contribution)

Reagents and Materials: $Bi(NO_3)_3.5H_2O$(Sigma-Aldrich, ≥ 98%), KBr (Himedia, 99.5%), ethylene glycol (L.R, 99%), bismuth (III) oxide (Bi_2O_3, Sigma-Aldrich, 99.99%), tantalum(V) oxide (Ta_2O_5, Sigma-Aldrich, 99.9%), rhodamine B(HPLC grade ≥ 95%), and ethanol(C_2H_5OH, ACS grade) were used as received without further purification. HPLC grade water was used while performing HPLC.

Characterizations: Rigaku Ultima IV diffractometer equipped with Cu Kα X-ray radiation with a wavelength of 1.5406 Aº (40 kV and 40 mA) was used to record Powder X-ray diffraction (XRD) patterns. The data were collected from 5 to 75 over 2θ with a scanning speed of 1degree/minute in 0.02 step. A field-emission scanning electron microscope (FESEM, JEOL, JSM-7600F, accelerating voltage of 20-30 kV), Atomic force microscope (AFM Park System XE7), and Transmission electron microscope (TEM (JEOL JEM-F200) were used to analyzed the morphology of the catalyst. Samples for SEM were prepared by drop-casting ethanolic dispersions of the sample on silicon wafers and allowing the solvent to evaporate slowly at room temperature in a vacuum desiccator. An aqueous dispersion of the material was drop casted on a holey carbon-coated Cu grid for TEM observation. The diffuse reflectance spectra (DRS) were recorded using a UV-Vis spectrophotometer (Cary 5000), using $BaSO_4$ powder as the reference. BET surface area was recorded by an autosorbiQ2 Quantachrome instrument (Autosorb Iq-c-XR-XR). The apparent surface area was calculated by the Bruner Emmett Teller (BET) method. Photoluminescence studies were carried out using spectrofluorometer (Horiba Scientific). Time-correlated single photon counting (TCSPC, Horiba Jobin Yvon, NJ) measurements were carried out employing 300 nm as excitation

wavelength, with a 375 nm laser diode used as a light source. The emission monochromator for RhB and Rh110 was fixed at 583 nm and 533 nm respectively with a bandpass of 4 nm. The instrument response function (IRF) was collected using Ludox (colloidal silica). The width (FWHM) of IRF was ~250 ps. The fluorescence lifetime traces were fitted bi-exponentially according to the following equation:

$$I(t) = A1 \exp(t/\tau_1) + A2 \exp(t/\tau_2)$$

UV-Vis absorption spectra were recorded using a Perkin Elmer UV-Vis Lambda 365 UV-Vis spectrophotometer at room temperature. The HRMS studies were carried out with Water Synapt G2-Si Q-TOF mass spectrometer using an electron spray ionization (ESI) positive mode of operation. RhB, intermediates and Rh110 formed during the photocatalytic process were analyzed with high-performance liquid chromatography (HPLC, Waters) equipped with 2998 array detector and Crest Pak C18 column in the mixed eluent (CH_3CN: H_2O = 1:1 by volume, ClO_4^-=150 mM, H_2PO_4 = 50 mM). X-ray photoelectron spectroscopy measurements were performed using AXIS ULTRA XPS spectrometer. The ^1H NMR spectra were recorded using a 400 MHz Bruker BioSpin Avance III FT-NMR spectrometer with TMS as the standard at room temperature and DMSO as solvent.

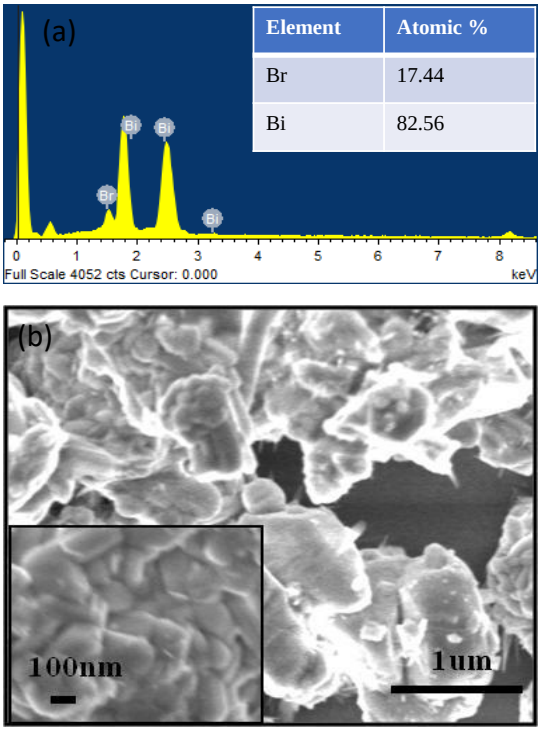

Figure S1: (a) SEM-EDS spectra of the samples confirming the presence of 35-40% of Bi_3TaO_7 phase in Bi_3TaO_7-Bi_4TaO_8Br heterostructures **(b)** FE-SEM image (inset is a high magnification image) of Bi_3TaO_7-Bi_4TaO_8Br heterostructures showing intergrowth particles having 100-500 nm feature sizes.

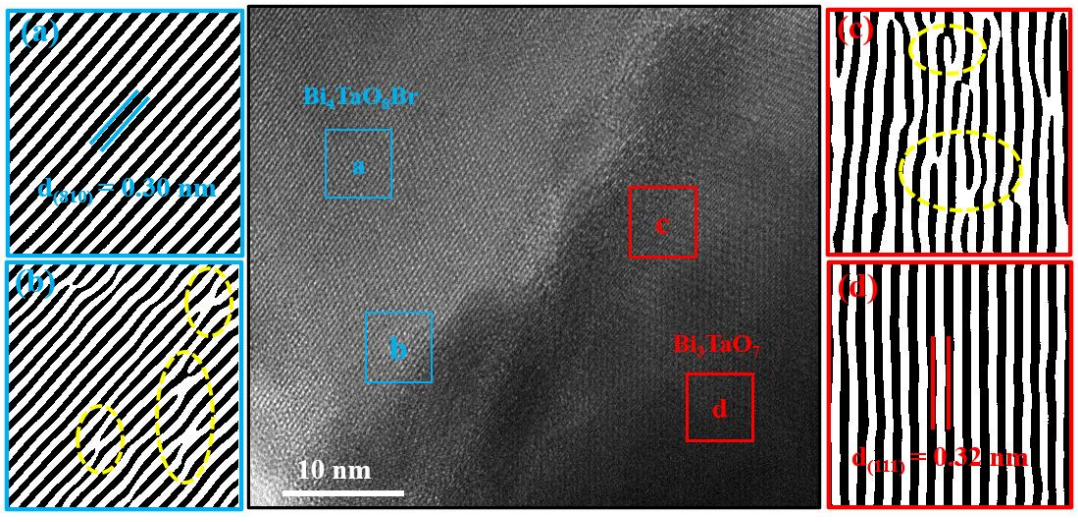

Figure S2: HRTEM image of the heterostructure and IFFT images corresponding to the different areas of heterostructure marked as boxes showing the defects near the junction of the two phases.

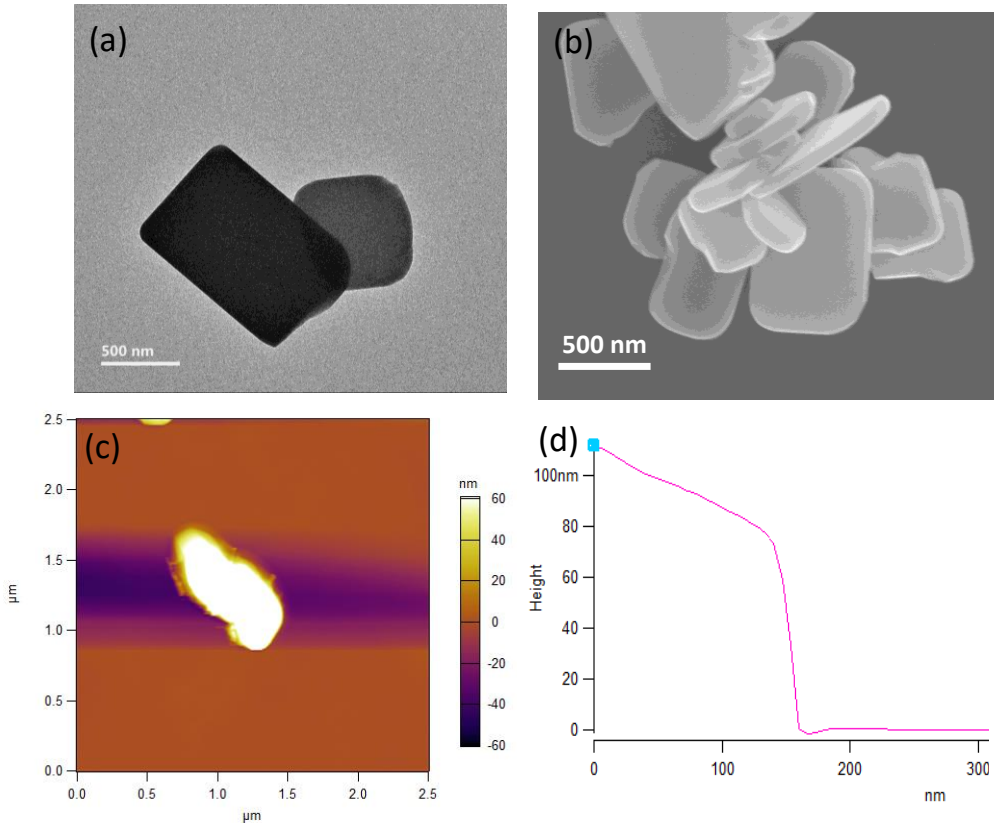

Figure S3: (a, b) HRTEM and FE-SEM images of Bi_4TaO_8Br obtained by flux method showing the formation of nanoplate with edges of several micrometres **(c, d)** AFM images and the corresponding height curves of Bi_4TaO_8Br with a thickness of ~100 nm.

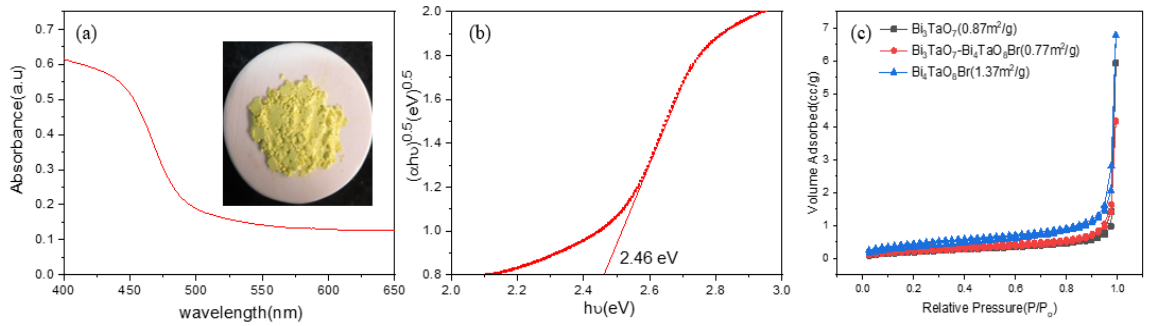

Figure S4: (a, b) UV-Vis DRS spectrum of the Bi_3TaO_7-Bi_4TaO_8Br heterostructures prepared in the air showing a steep absorption edge beginning from 510 nm and extending beyond 400 nm consistent with its intense yellow colour (inset). The corresponding optical bandgap was estimated from Tauc analysis using the equation (1).

$$(\alpha h\nu) = A\,(h\nu - Eg)^{n} \quad \ldots\ldots\ldots\ldots (1)$$

where A = constant, hν = light energy, Eg = optical bandgap energy, n = 2 considering an indirect bandgap and α = absorption coefficient. From the corresponding Tauc plot, a bandgap of the heterostructure was estimated to be 2.46 eV. **(c)** The specific surface areas of pure Bi_3TaO_7, Bi_4TaO_8Br and Bi_3TaO_7-Bi_4TaO_8Br heterostructures were measured by nitrogen sorption at 77 K and calculated by the Brunauer–Emmett–Teller (BET) method.

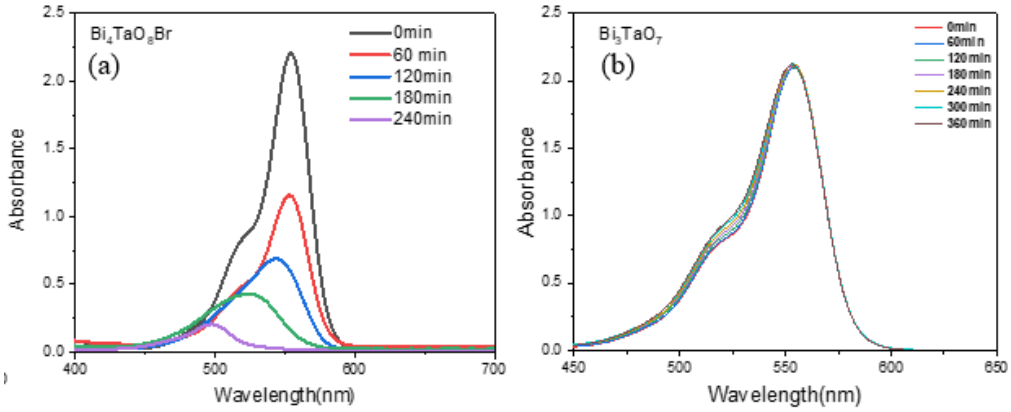

Figure S5: UV-Vis. absorption spectra recorded during photocatalytic conversion of RhB to Rh110 over (a) pure Bi_4TaO_8Br and (b) Bi_3TaO_7. The yields of pure Rh110 are 13% for Bi_4TaO_8Br and negligible for Bi_3TaO_7.

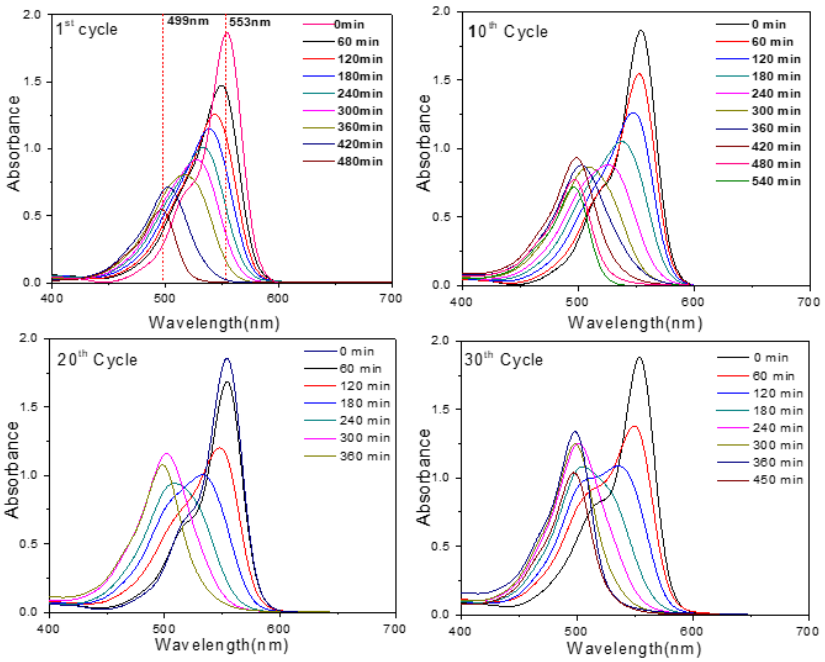

Figure S6a: UV-Vis. absorption spectra showing an increase in the yield of Rh110 over Bi_3TaO_7-Bi_4TaO_8Br heterostructures synthesized in the air atmosphere with continuous use of the catalyst up to the 30th cycle.

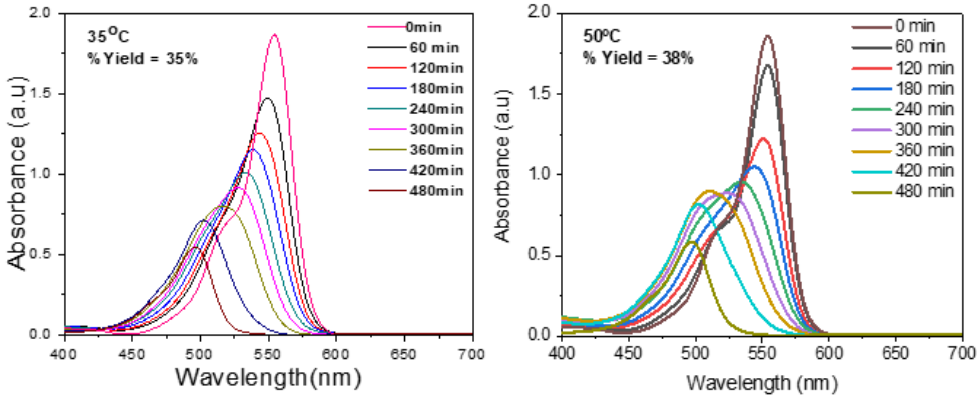

Figure S6b: As we carried out the experiments both in natural sunlight (which can have a temperature range of 35-45 ^{o}C) and benchmarked them using a solar simulator, we have checked Rh110 yield at two different temperatures i.e., 35^{o}C and 50 ^{o}C. Figure shows the UV-Vis absorption spectra for RhB to Rh110 conversion at 35 and 50 ^{o}C respectively. Yields are 35% and 38% respectively. The slight difference in the yields is within the error bar.

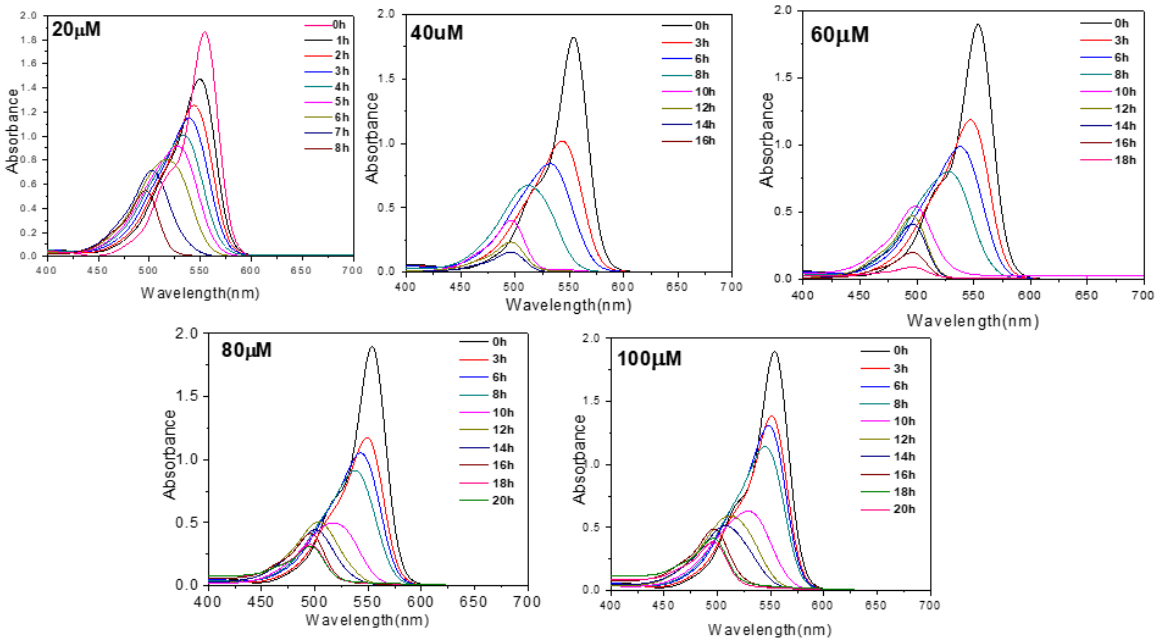

Figure S7: UV-Vis. absorption spectra recorded for different concentrations (20, 40, 60, 80, and 100 µM) of RhB solution with the same amount of the catalyst (40 mg) and the volume of RhB solution (25 ml). Note that the solutions were appropriately diluted before recording the spectra.

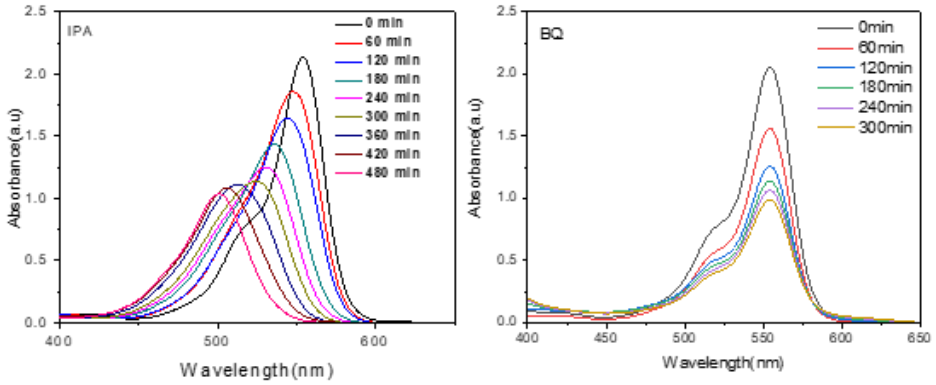

Figure S8: Evolution of UV-Vis spectra during photocatalytic conversion of RhB to Rh110 in the presence of isopropyl alcohol (IPA) and benzoquinone (BQ) as hydroxide and superoxide racial scavengers respectively.

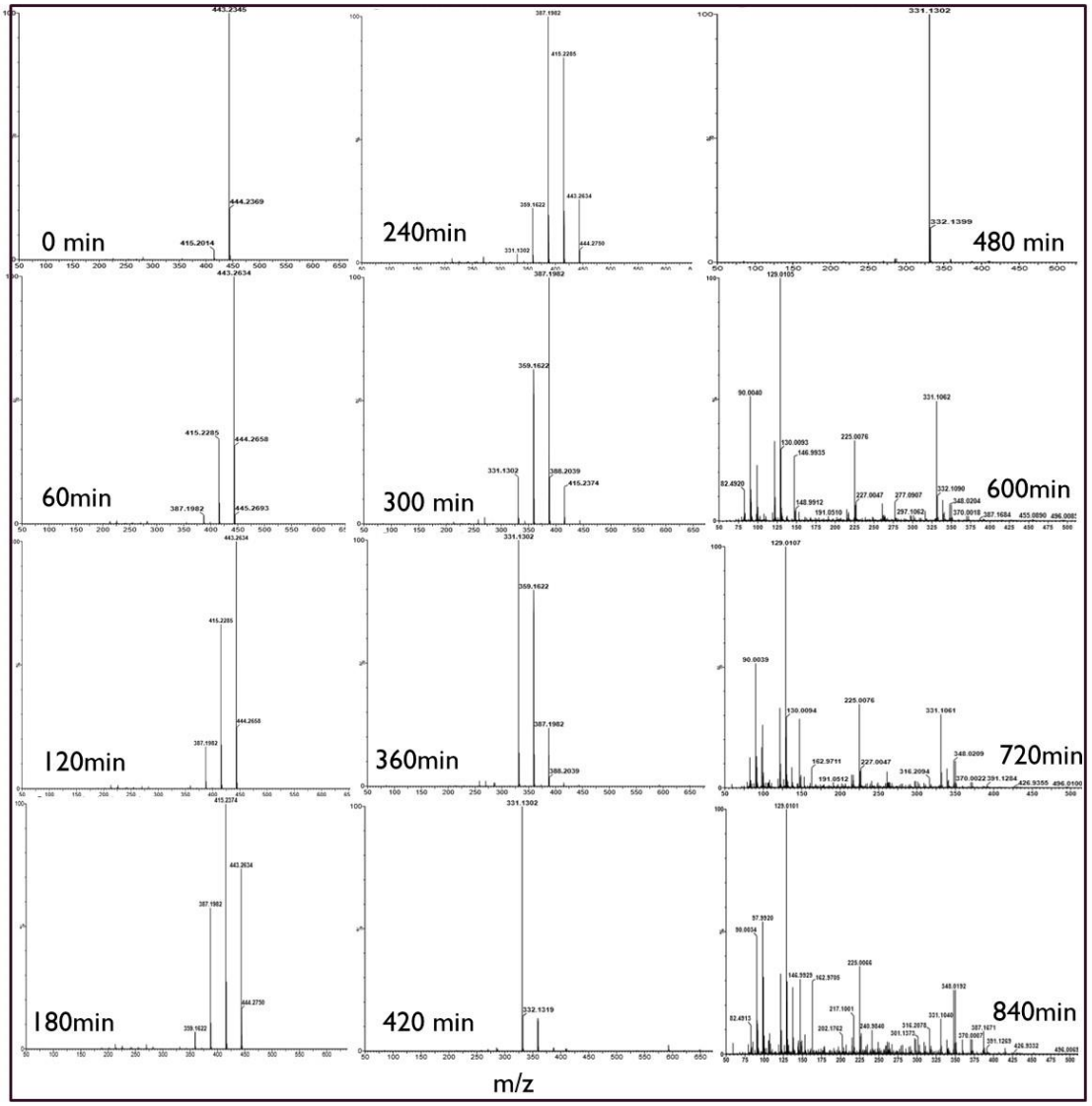

Figure S9: HRMS spectra recorded in the positive ion mode (ESI) during the photoirradiation of RhB in the presence of Bi_3TaO_7-Bi_4TaO_8Br heterostructures confirming step-wise deethylation of RhB to Rh110 and its further cleavage to small molecules after 480 min of photoirradiation.

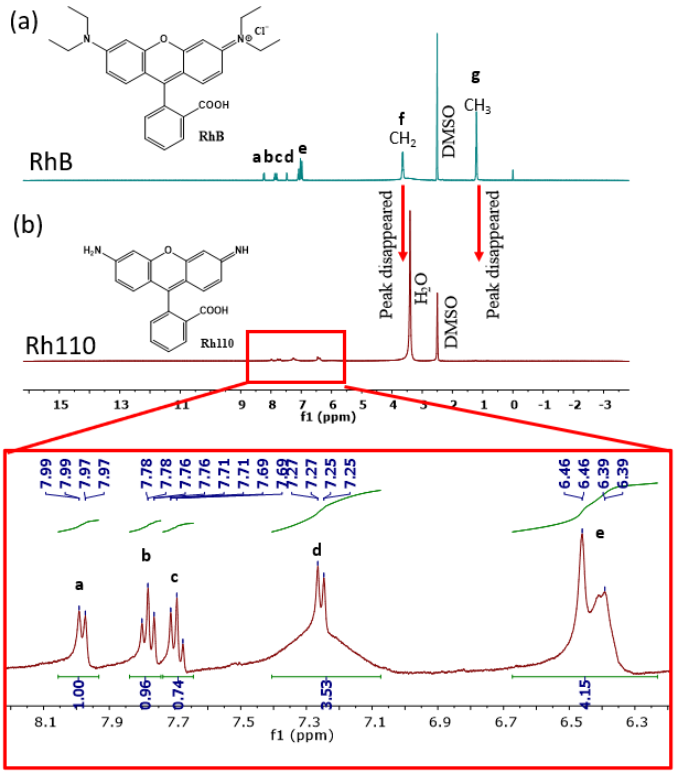

Figure S10 (a, b): H-NMR spectra for RhB and its de-ethylated product Rh110 in DMSO respectively. The NMR signals of the aromatic hydrogens H_a, H_b, H_c, H_d, and H_e are located at σ of 7.99-7.96, 7.80-7.76, 7.71-7.68, 7.27-7.25, and 6.46-6.39 ppm, respectively. H_f and H_g at σ of 3.65-3.64 and 1.22-1.19 ppm respectively representing the N-diethyl group of RhB which disappear after 480 min of light irradiation to confirm the formation of RH110.

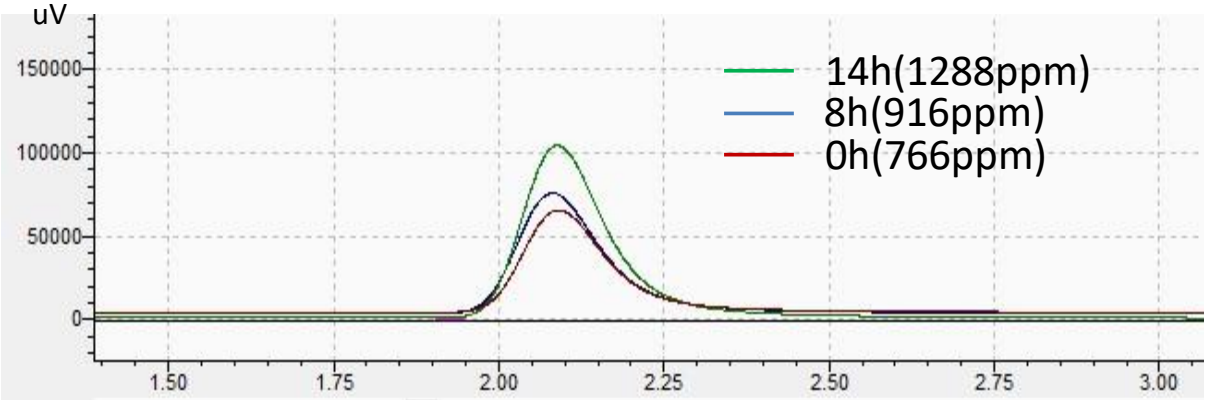

Figure S11: Gas chromatogram obtained from photocatalytic mineralization of RhB by Bi_3TaO_7-Bi_4TaO_8Br heterostructures under an oxygen atmosphere in the sealed reaction vessel during continuous photoirradiation confirming mineralization of RhB and its de-ethylated products. The peaks correspond to CO_2.

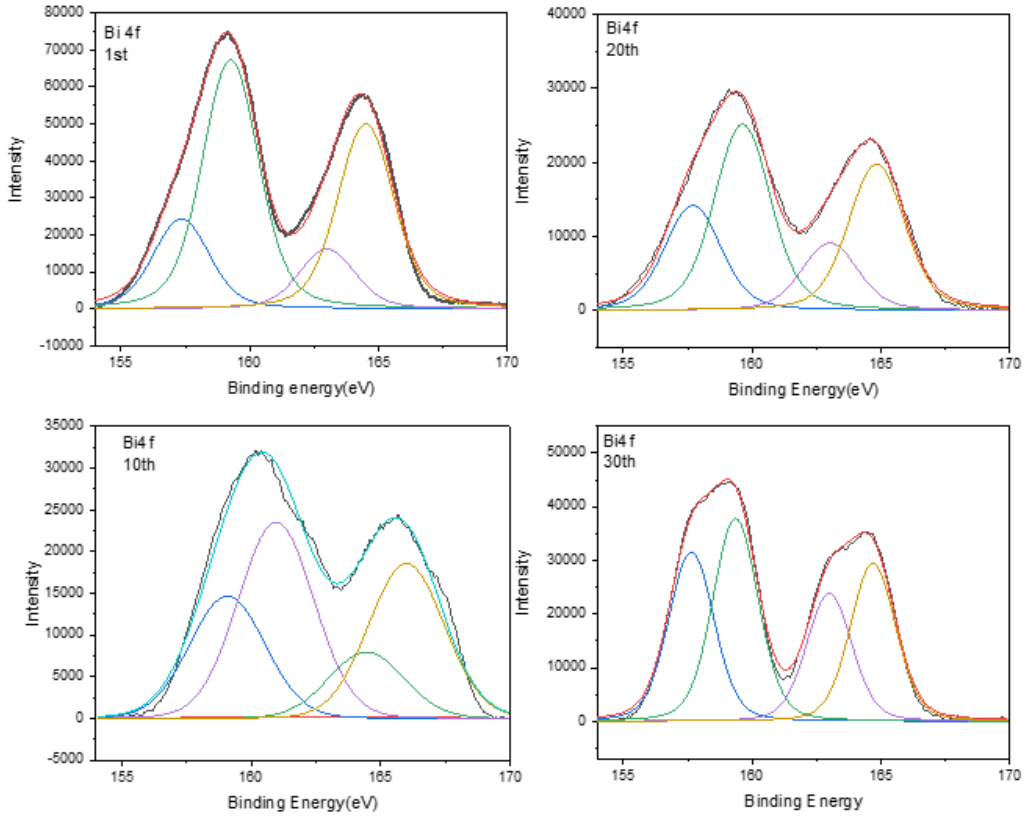

Figure S12: High-resolution Bi-4f XPS spectra of the used catalyst recorded after the 1st ,10th, 20th and 30th cycle.

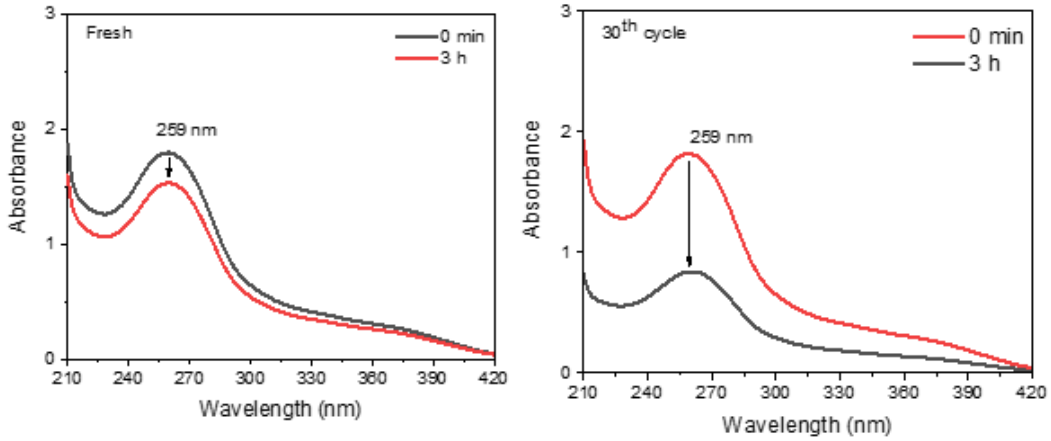

Figure S13: UV-Vis absorption spectra of NBT solution over fresh and used catalyst under light irradiation.

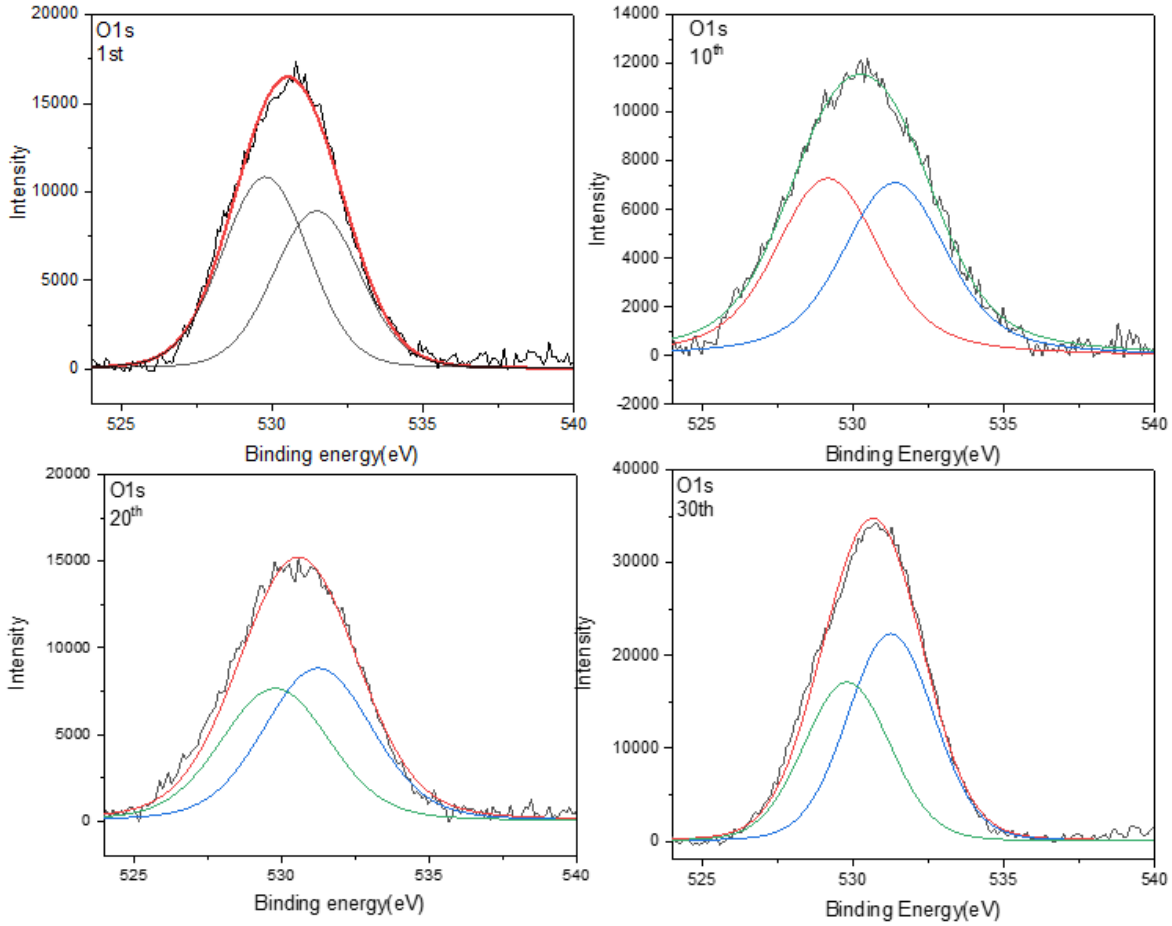

Figure S14: High-resolution O-1s XPS spectra of the used catalyst recorded after the 1st ,10th, 20th and 30th cycle catalyst.

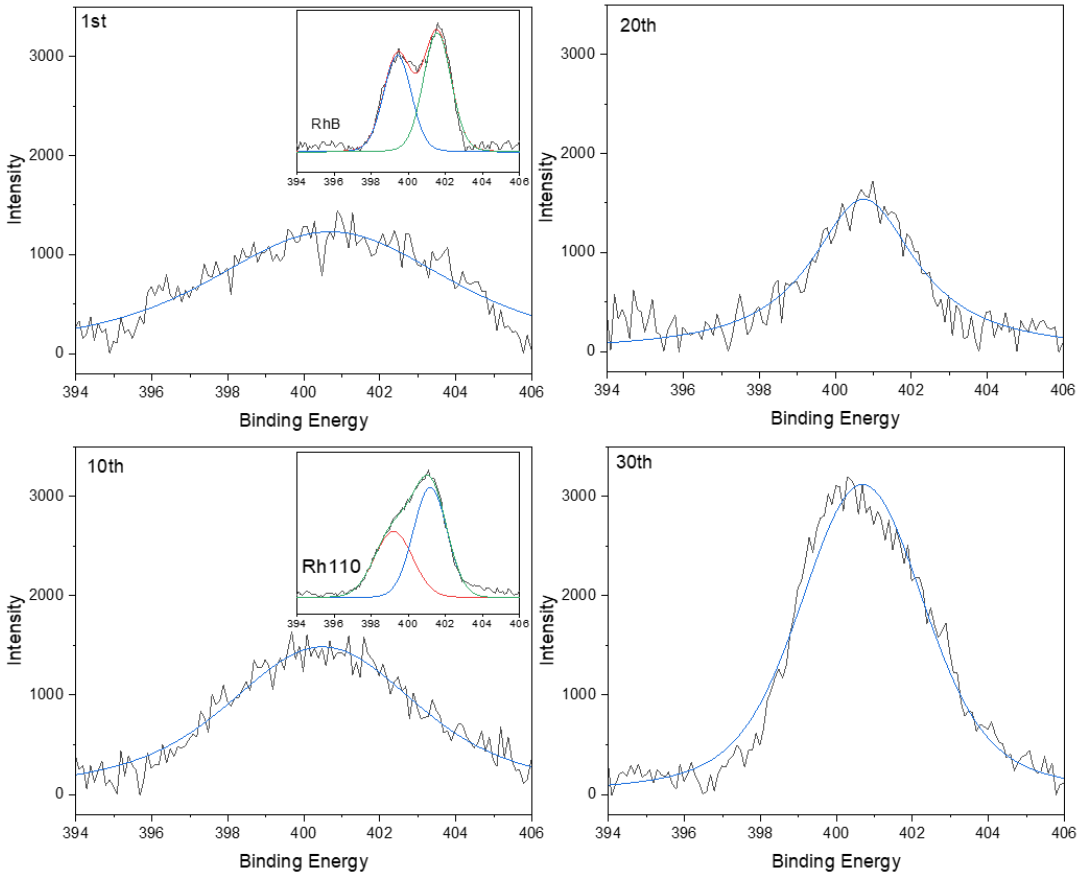

Figure S15: High-resolution N-1s XPS spectra of the used catalyst recorded after the 1st, 10th, 20th and 30th cycle catalyst.[1] Insets show the N-1s XPS spectrum of pure Rhodamine B and Rhodamine 110.[2]

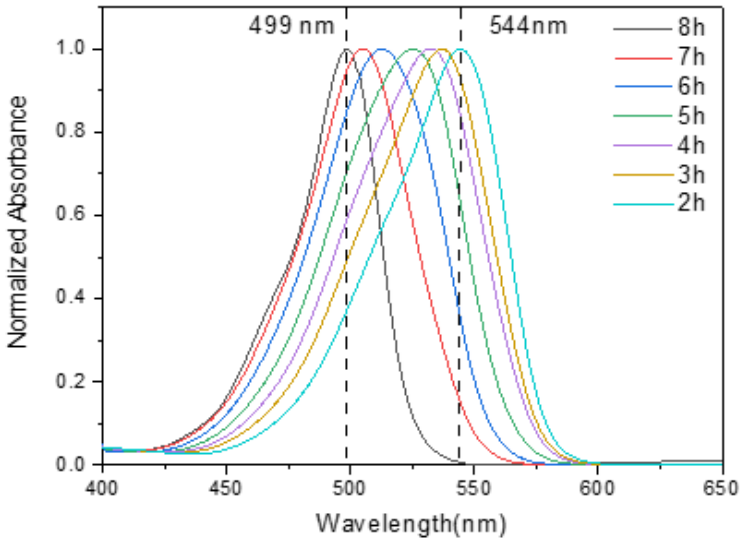

Figure S16: UV-Vis. absorption spectra of the extracted dyes from the catalyst surface.

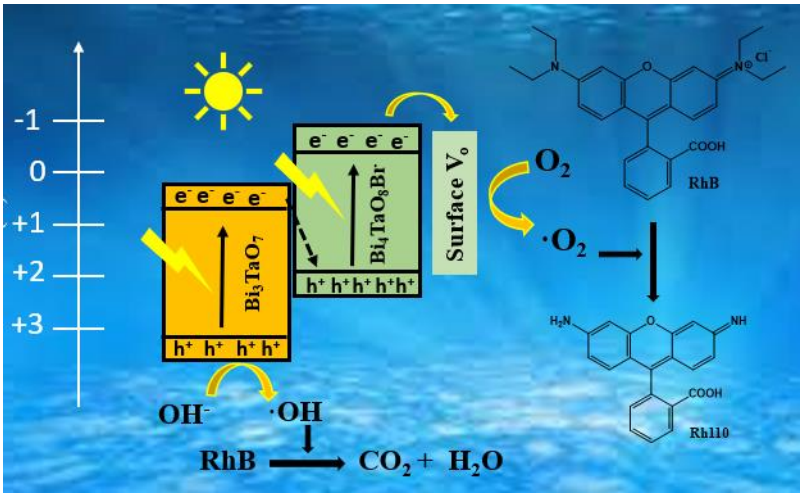

Figure S17: Schematic illustration of band-alignment and photoinduced electron transfer in the Bi_3TaO_7–Bi_4TaO_8Br composite for RhB to Rh110 conversion.

(**Note on the schematic in Figure S17**: The heterostructure contains the coexistence of two photoactive phases, Bi_3TaO_7 and Bi_4TaO_8Br and it leads to electron transport routes that resemble the Z-scheme. Conduction band (CB) of Bi_3TaO_7 is in the region of 0.32–0.46 V *vs*. NHE, while its valence band (VB) is in the range of 3.12–3.22 V. Similarly, the CB minima and VB maxima for Bi_4TaO_8Br were found to be 0.79 V and 1.74 V, respectively, vs. NHE.[4] The bandgaps calculated from the locations of CB and VB in these materials are quite similar to the value we determined experimentally. Furthermore, because the band locations in these two materials are so dissimilar, slight alterations in their actual placements are unlikely to affect the proposed scheme. When light shines on the sample, both the photoactive phases absorb

photons with energy hν matching with the bandgap, and then electrons from the valance band are moved to the conduction band, leaving behind holes in the valance band. The photo-generated electrons on the CB of Bi_3TaO_7 could transfer to the VB of Bi_4TaO_8Br and quench the holes of Bi_4TaO_8Br, effectively inhibiting the recombination of the electron-hole pairs in both Bi_3TaO_7 and Bi_4TaO_8Br. Furthermore, it is observed from the XPS spectroscopy that there is a large density of surface oxygen vacancy sites on the catalyst surface and these vacancies play an important role as a carrier trapping center. The trapped electrons on the surface V_O produce superoxide radicals through the reduction of oxygen molecules. Then, these radicals (the main active species responsible for deethylation) react with RhB and deethylate it into Rh110. Holes available in the VB of Bi_3TaO_7 could directly react with OH^- ion and form ·OH which is responsible for chromophore cleavage of RhB.

Supporting Note -1

Apparent Quantum Efficiency (AQE): The apparent quantum yield (AQE) for photocatalytic deethylation of RhB was calculated by carrying out the reaction under a solar simulator (Verasol Newport) with a conversion of 35% within 480 min. For calculation of AQE, we counted the number of incident photons from higher energies till 500 nm, where, based on the UV-Vis absorption spectrum of Bi_3TaO_7-Bi_4TaO_8Br, the absorption is >98%. The incident power ($P_{incident}$ (λ)) on the sample can be represented as[3]:

$$P_{incident}(\lambda) = \rho_{incident}(\lambda) \times A(sample) \quad \text{---------- (i)}$$

A(sample) is the area exposed to incident light (12.56 cm^2), $\rho_{incident}$ (λ) is the incident power for a photon of wavelength λ, which is obtained from the solar simulator spectrum plotted (**Figure S18**) as irradiance vs. wavelength.

The number of incident photons per second, as a function of wavelength can be expressed as:

$$N_{ph}(\lambda) = \frac{\rho_{incident}}{E_{ph}(\lambda)} \quad \text{---------- (ii)}$$

Where $$E_{ph}(\lambda) = \frac{hc}{\lambda} \quad \text{---------- (iii)}$$

E_{ph}(λ) is the photon energy for the corresponding λ. The total number of photons incident on the sample per second within the wavelength range of 400-500 nm can be calculated as:

$$N_{ph,incident}(400-500) = \int_{400}^{500} \frac{\rho_{incident(\lambda)}}{\lambda hc} d(\lambda) \quad \text{---------- (iv)}$$

(Considering the units for $\rho_{incident}(\lambda)$ as W/m^2. nm and length units in nm)

$$= \int_{400}^{500} \frac{\rho_{incidenent} \times \left(\frac{W}{m^2.nm}\right) \times \lambda(\text{nm})}{6.63\times10^{-34}\ J.S \times 3\times10^{8}\times10^{9} nm.s^{-1}} \times d\lambda(\text{nm})$$

$$= \int_{400}^{500} \frac{\rho_{incident}}{19.89\times10^{-17} m^2.s} \times d(\lambda)$$

In terms of moles:

$$= \int_{400}^{500} \frac{\rho_{incident}(\lambda)\times\lambda}{19.89\times10^{-17}\times6.023\times10^{23} mol^{-1}.m.s} d\lambda$$

$$= \int_{400}^{500} \frac{\rho_{incident} \times \lambda}{0.12 \times 109 mol^{-1}.m^2.s} d\boldsymbol{\lambda}$$

$i.e.$ $\int_{400}^{500} \frac{\rho_{incident} \times \lambda}{0.12 \times 109 mol^{-1}.m^2.s} d\boldsymbol{\lambda}$ moles per second per square meter

= 0.006556 moles per second per square meter

The number of incident photons in the reaction mixture within the reaction time

$= N_{ph,incident}$ (400 − 500) × Asample × $Reaction\ time$ ---------- (v)

= 0.175×10^{-6} moles in our reaction

The AQE can be derived from the following equation:

$$AQE = \frac{n(No.of\ electron) \times No.of\ moles\ of\ RhB \times \%\ conversion}{Number\ of\ incident\ photons} \times 100(\%)$$ -------(vi)

For RhB to Rh110 conversion, we considered n as 8 (Formation of a superoxide radical requires one electron while two superoxide radicals are needed for the removal of one ethyl group)[5]

No. of moles of RhB × %conversion = 0.05×10^{-6} moles × (35%) = 0.175×10^{-6} moles

Thus, for 400-500 nm:

$$AQE = \frac{8 \times 0.175 \times 10^{-6}}{0.006556} \times 100\ (\%) = 0.02\ \%$$

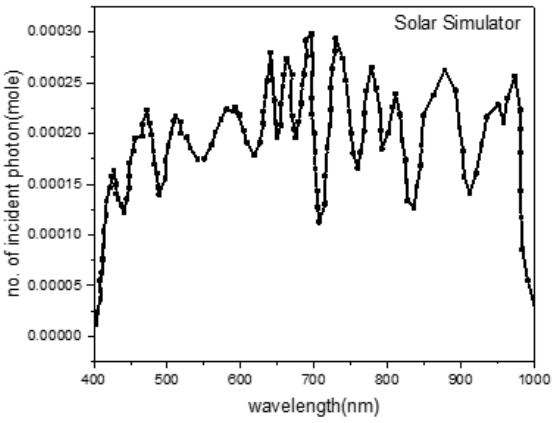

Figure S18: Spectrum of the solar simulator.

Supporting Note 2 (on scale up): The large-scale production should be considered by comparing photocatalytic experiments of any colored samples where the concentration plays a barrier since at high concentration, light penetration is poor. We have shown the potential of up to ~20 mg of Rh110 per cycle (by considering 60% yield as average, 1 L RhB solution of 100 μM). We have shown up to 5-time increase in RhB concentration without compromising efficiency and tested catalyst recyclability up to 30 cycles inferring we can convert 1437 mg of RhB to 658 mg of Rh110 (~2 mmol). This should be compared with 0.2 mg of RhB studies currently in practice. Therefore, from our control experiments, it is clear that we have made significant progress of ~4000 times scaleup.

References:

(1) L. F. Vieira Ferreira, P. V. Cabral, Almeida, A. S. Oliveira, M. J. Reis, A. M Botelho Do Rego, *Macromolecules* **1998**, *31*, 3936.

(2) Q.Wang, Chen, C.; D. Zhao, M. Wanhong, J. Zhao, *Langmuir* **2008**, *24*, 7338.

(3) S. Mondal, S. R. Das, L. Sahoo, S. Dutta, U. K. Gautam, *J. Am. Chem. Soc.*, **2022**, https://doi.org/10.1021/jacs.1c10636.

(4). Chatterjee, K., Banoo, M., Mondal, S., Sahoo, L. & Gautam, U. K. *Dalt. Trans.* 2019, **48**, 7110.

(5) O. Merka, V. Yarovyi, D. W. Bahnemann, M. Wark, *J. Phys. Chem. C* **2011**, *115*, 8014.